To be published in Photonics Research:

Title: Ultra-broadband Flat-top Quantum Dot Comb Lasers

Authors: Jing-Zhi Huang,Zitao Ji,jiajian chen,Qi Wei,Jiale Qin,Zhiyuan Li,Zihao Wang,Ting Wang,xi xiao,Jianjun Zhang

Accepted: 17 March 22

Posted 18 March 22

DOI: https://doi.org/10.1364/PRJ.446349

OPTICA
PUBLISHING GROUP
Formerly OSA

Ultra-broadband Flat-top Quantum Dot Comb Lasers

JING-ZHI HUANG,[1,2,†] ZI-TAO JI,[4,†] JIA-JIAN CHEN,[1,2] WEN-QI WEI,[3] JIA-LE QIN,[1,2] ZI-HAO WANG,[1,2,3,6] TING WANG,[1,2,3,8] ZHI-YUAN LI,[4] XI XIAO,[5] AND JIAN-JUN ZHANG[1,2,3,7]

[1]*Beijing National Laboratory for Condensed Matter Physics, Institute of Physics, Chinese Academy of Sciences, Beijing 100190, China*
[2]*Center of Materials Science and Optoelectronic Engineering, University of Chinese Academy of Science, Beijing 100049, China*
[3]*Songshan Lake Materials Laboratory, Dongguan, Guangdong 523808, China*
[4]*School of Physics and Optoelectronics, South China University of Technology, Guangzhou, Guangdong 510641, China*
[5]*National Information Optoelectronics Innovation Center, China Information and Communication Technologies Group Corporation (CICT), Wuhan, Hubei 430074, China*
[6]*Email: wangzihao@iphy.ac.cn*
[7]*Email: jjzhang@iphy.ac.cn*
[8]*Email: wangting@iphy.ac.cn*

OPTICA PUBLISHING GROUP Formerly OSA

Quantum dot (QD) mode-locked laser as an active comb generator takes advantage of its small footprint, low power consumption, large optical bandwidth, and high-temperature stability, which is an ideal multi-wavelength source for applications such as datacom, optical interconnects, and LIDAR. In this work, we report 4th order colliding pulse mode-locked laser (CPML) based on InAs/GaAs QD gain structure, which can generate ultra-stable optical frequency combs (OFCs) in O-band with 100 GHz spacing at operation temperature up to 100 °C. A record-high flat-top optical comb is achieved with 3 dB optical bandwidth of 11.5 nm (20 comb lines) at 25 °C. The average optical linewidth of comb lines is measured as 440 kHz. Single channel non-return-to-zero (NRZ) modulation rates of 70 Gb/s and four-level pulse amplitude modulation (PAM-4) of 40 GBaud/s are also demonstrated. To further extend the comb bandwidth, an array of QD-CPMLs driven at separate temperature is proposed to achieve 36 nm optical bandwidth (containing 60 comb lines with 100 GHz mode spacing), capable of a total transmission capacity of 4.8 Tbit/s. The demonstrated results show the feasibility of using QD-CPML as a desirable broadband comb source to build future large-bandwidth and power-efficient optical interconnects.

1. INTRODUCTION

The generation of optical frequency combs (OFCs) are of recently great interest as they can provide equidistant mutually locked coherent modes which make them as ideal sources for precision metrology, data communications, and optical interconnects. Over the past decades, various approaches have been extensively investigated to realize on-chip OFCs, such as IM/Phase EO modulation [1-3], soliton microresonators [4-6], gain-switched combs [6,8], and passive mode-locked lasers (MLLs) [9]. Among them, soliton microresonators have drawn significant attentions recently due to their compactness and ultra-wide bandwidth. In comparison, semiconductor MLLs have advantages of electrically driven, while do not require external high-power optical pumping which makes them a great candidate for highly efficient, small-footprint and low power consumption solutions for optical time division multiplexing (OTDM) [10] and wavelength division multiplexing (WDM) systems [10]. Recent years, there have been significant attentions paid to quantum dash (Q-dash) [11-13] and quantum dot (QD) MLL [9,15,16] as flat-top comb source, due to their properties of small linewidth enhancement factor (LEF), fast carrier dynamic

induced self-frequency modulation and defect insensitivity, which make them an ideal platform for reflection insensitive [16,18], temperature insensitive [19,20], and most importantly, direct-grown-on-Si light source [21-25].

Conventionally, semiconductor MLLs have been investigated to produce the optical pulses with a wide range of repetition rates from MHz to hundreds of GHz as listed in Table 1. The ultra-dense optical combs (repetition rate < 1 GHz) leads to applications for sensing or spectroscopy [26], however, for WDM communication applications, small repetition rate, which also corresponds to narrow channel spacing of WDM system, are limiting the highest modulation bandwidth of each channel due to strong crosstalk [28]. Currently, the minimum channel spacing requirement of CW-WDM MSA [29] is 100 GHz. Considering that the typically used NRZ modulation speed nowadays is around 100 Gbps, MLL with at least 100 GHz mode spacing is required for large bandwidth data transmission. The bandwidth of flat-top OFC is another figure of merit for WDM system which is strongly dependent on the 3 dB optical bandwidth. It is suggested that quantum dot (QD) MLLs have larger 3 dB bandwidth compared with the quantum well (QW) systems due to their physical nature of broad gain spectrum [9,30].

Table 1. Comparison of mode-locked comb laser on various material platforms and structures

	Mode-locking mode	Material platform	Repetition rate GHz	Optical bandwidth nm	Optical linewidth kHz	Operating temp. °C
[26]	Anti-CPM (External Cavity)	InGaAsP MQWon Si	1	12 (-10dB BW)	400	20
[26]	Hybrid Anti-CPM (External Cavity)	InGaAsP MQW on Si	1	13 (-10dB BW)	400	20
[31]	CPM (External Cavity)	InGaAsP MQW on Si	10	6.4 (-3dB BW)	>15	16
[32]	CPM (External Cavity)	MQW on Si	20	2.96(-3dB BW)	NA	NA
[33]	Two-section	InAs/GaAs QD on Si	20	6.1 (-3dB BW)	10000	18
[34]	Two-section	InAs/GaAs QD	25.5	4.7(-6dB BW)	NA	20-120
[35]	Two-section	AlGaInAs/ InP MQW	100	8.05(-3dB BW)	NA	20
[36]	CPM (External Cavity)	InAs/GaAs QD on SOI	102	6.5(-3dB BW)	NA	25
[37]	CPM (External Cavity)	InAs/GaAs QD on SOI	15.5	12(-3dB BW)	NA	23
This work	**4th order CPM**	**InAs/GaAs QD**	**100**	**11.5(-3dB BW)**	**440**	**25-100**

In this work, we experimentally demonstrate an O-band 100 GHz InAs/GaAs QD-CPML (4th order) with a record wide 3 dB optical bandwidth of 11.5 nm and a state-of-art working temperature ranging from 20 °C to 100 °C. By optimizing the operation conditions, we have achieved steady flat-top ML region of 20 comb lines within 3 dB optical bandwidth at 100 GHz mode spacing. The individual comb lines exhibit narrow average optical linewidth of 440 kHz. The measured relative intensity noise of the entire comb spectrum and each channel are -160 dB/Hz and -133 dB/Hz in the frequency range from 10 MHz to 20 GHz, respectively. The MLLs have also shown reasonable over-time wavelength drifting of approximately 200 MHz and 1 GHz for 10 minutes and 20 hours stability examinations. The high-speed large-signal modulation experiment has been performed on each of 20 comb lines, while open eyes are obtained for both 70 Gb/s NRZ and 40 GBaud/s PAM-4 modulation rates, which indicate the QD-CPML have capability to transmit at 1.6 Tbit/s with single comb laser. To further increase the data transmission bandwidth, upgraded solution is proposed here by using four QD-CPMLs operated at separately

OPTICA PUBLISHING GROUP Formerly OSA

adjusted temperature. Over 36 nm wide comb spectrum with 100 GHz grid is obtained which can generate at least 60 comb lines for 4.8 Tbit/s transmission capacity.

To place our demonstration in to context, the performance analysis of mode-locked comb lasers on various platforms have been compiled in Table 1. For external cavity MLLs, QW lasers exhibit relatively narrow optical linewidth, benefitting from their long cavity length [26, 31,32,36,37]. But the repetition rates (comb spacings) are also limited within 20 GHz. In contrast, short cavity two-section MLLs, which have a single saturable absorber at the end of the cavity, would be able to produce comb lines with larger channel spacing, but the optical linewidth is normally within the range of tens of MHz [33]. In addition, high repetition rate two-section MLs do also experience low optical gain due to its short cavity property, which leads to a significant degradation in single channel output power. Here, by incorporating high-order CPM technique, we could generate 100 GHz grid comb laser with ultra-wide optical bandwidth (11.5 nm), while retaining 1580 μm cavity length for sufficient output power.

2. DEVICE DESIGN AND FABRICATION

The epitaxy of QD-CPML is grown by molecular beam epitaxy (MBE) on an n-type GaAs (100) substrate, containing 8 stacks of self-assembled InAs QD layers. The active region of dots in well (DWELL) structure is p-doped to improve the high-temperature stability of the lasers. A symmetric cladding layer design is used by utilizing 1500 nm thick p-type and n-type $Al_{0.4}Ga_{0.6}As$ for upper and lower cladding layers, respectively. In order to achieve 100 GHz repetition rate, ultra-short laser cavity length of approximately 400 μm is normally required, which encounters significant gain reduction issues limiting the maximum output power of individual comb lines. To remain sufficient gain area, while keeping large mode spacing, here, we introduce high-order CPML design to overcome the insufficient gain issue. The schematic of 4th order QD-CPML is shown in Fig. 1(a). The total distance of the laser cavity is four times longer than the two-section MLL which produces pulses with fundamental repetition rate. In order to produce 100 GHz spacing OFCs, the cavity length of fundamental mode is calculated as ~395 μm by using an effective group index of 3.8. Considering that QDs lasers with such a short cavity may not have enough gain to support stable mode-locking and decent output power, 4th order MLL design with 1580 μm cavity length is implemented here to allow four colliding pulses traveling intracavity to produce 4th order harmonic pulses at 100 GHz repetition rate. As shown in Fig. 1(a), three saturable absorbers (SAs) equally divide the entire laser cavity with four gain sections, while all the SAs and gain sections are electrically connected through probe metal layers to simplify the measurement. There has been high order harmonic design of two SAs applied in the front and rear of the laser facets [38], as we found the evenly distributed SAs could produce more stable high-order harmonic mode-locking combs. To suppress the losses induced from extra SAs included here, the overall length of three SAs is chosen as 10% of the total cavity length, slightly shorter than the conventional design (usually 15 - 20%).

The QD-CPMLs are fabricated with ridge waveguide and mesa widths of 4 μm and 25 μm, respectively. The three SAs are equally spaced along the cavity with the length of 50 μm, where the electrical isolation gap next to the SA is designed as 10 μm wide. The QD-CPML is then fabricated in line with the standard ridge waveguide InAs QD lasers by using dry etching, dielectric passivation and metal contact deposition. The electrical isolation gaps are simultaneously defined with ridge waveguide etching by carefully control the dry etching depth at 100 nm above the active region. This process simply avoids additional efforts made to the sperate definition of isolation trenches. The detailed fabrication processes are discussed in our previous work [23,24]. The SEM picture in Fig. 1(b) shows the fabricated QD-CPML device, where the inset shows the zoom-in isolation gap region between gain section and SA. The sheet resistance is ~30 kΩ measured through I-V characteristics, which provides enough electrical isolation between SAs and gain

OPTICA PUBLISHING GROUP Formerly OSA

sections. After device process, the laser die is mechanically thinned to 105 μm and cleaved into laser bars without high-reflection coating for this work.

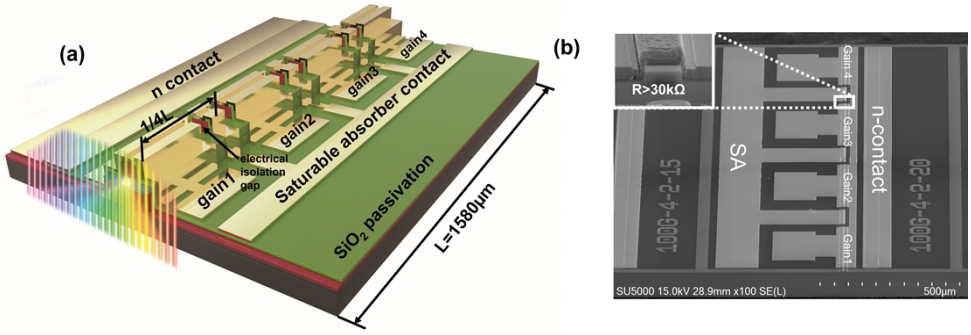

Fig. 1. (a) Schematic of InAs/GaAs 4th order CPML design (total cavity length of 1580 μm) with four gain sections (360 μm for each section) and three equally spaced saturable absorber (50 μm for each SAs). (b) Cross-section SEM image of a fabricated device with a 45° tilted angle. Inset: Magnified SEM image on electrical isolation trench region.

3. DEVICE CHARACTERIZATIONS AND DISCUSSIONS

The fabricated QD-CPML is mounted on an AlN chip-on-carrier (CoC) for heat dissipation, while all the SAs, gain sections and n contact pads are wire bonded to the COC with three separated pads. The QD-CPML CoC is then mounted on top of a thermoelectric cooler (TEC) for constant temperature control. The gain sections are driven by Keithley 2520 current source and SAs are reverse biased by a voltage source. By using an integration sphere with an InGaAs photodetector to collect optical output power from lasers, the light-current (L-I) performance of QD-CPML was characterized as shown in Fig. 2(a).

The lasers are characterized with gain current (I_g) ranging from 0-200 mA and SA reverse biased (V_{SA}) from 0 to -5 V under wide temperature variation from 20 °C to 100 °C. It shows that the QD-CPML could operate at high temperature of 100 °C and still exhibit optical power over 15 mW at condition I_g = 200 mA and V_{SA} = 0 V. Among all reverse bias conditions, the characteristic temperature is always larger than 110 K at temperature from 20 °C to 70 °C. This temperature resilience performance is contributed to the p-doped active region of QD lasers [39, 40]. At fixed temperature condition, the increment of reverse biased SA voltage causes the decreased optical output power and elevated threshold current. For example at 20 °C, as V_{SA} increased from 0 V to -5 V, the optical power dropped from 32 mW to 28 mW. In addition, the threshold current increases slightly from 29 mA to 36 mA, which is mainly caused by the higher cavity losses induced from SAs. Noticeably, under reverse bias conditions, the L-I curve shows the abrupt kink around threshold, which is caused by the nonlinear saturation effect of SAs [15,34]. These effects are enhanced at high reverse biased voltage (V_{SA} = -5 V) and high temperature operation (90 °C) due to the strong absorption from SAs and simultaneous gain degradation at high temperature. Fig. 2(b) shows the temperature dependent optical spectral evolution of QD-CPML from 20 °C to 100 °C at optimum operation conditions. The operation conditions marked at each temperature are slightly adjusted to achieve flat-top combs. It is noted that the 3 dB optical bandwidth does not dramatically narrow as temperature increased, which indicates the stable operation of flat-top combs. Even at high temperature operation of 80 °C, 3 dB bandwidth of 11.3 nm can still be achieved, which is the widest flat-top OFCs reported at high temperature to the best of our knowledge. The broadband comb source only starts to degrade at 100 °C in line with the rolled-over L-I curves, in which case the laser can only generate 3.8 nm wide comb lines under optimized operation conditions. Interestingly, an ultra-flat comb spectrum with just 0.8 dB variation between 14

OPTICA PUBLISHING GROUP Formerly OSA

combs is achieved at 80 °C. We suspect that this phenomenon is caused by ideal dispersion compensation at this specific operation point [41].

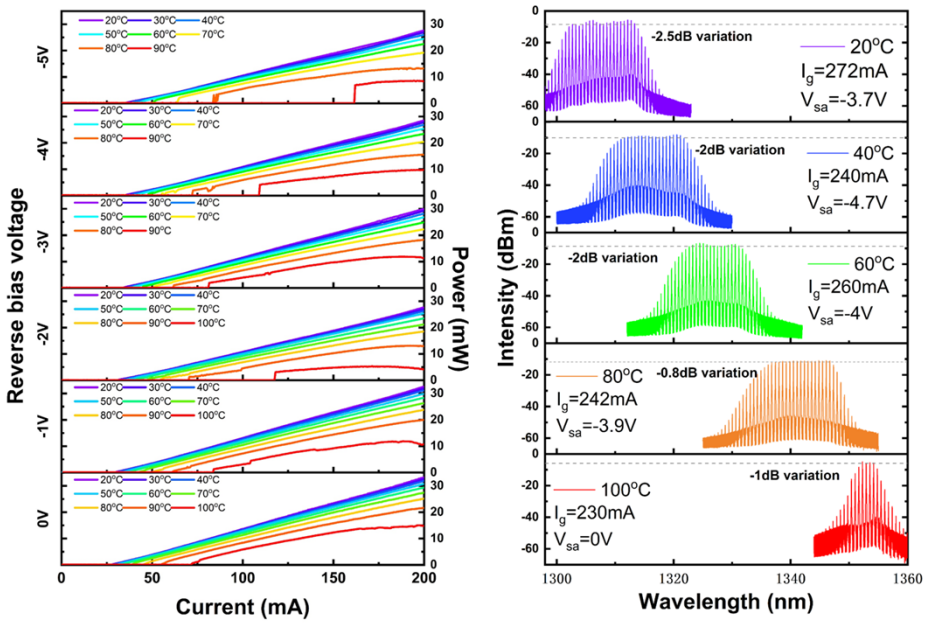

Fig. 2. (a) Temperature dependent continuous-wave light current (L-I) characteristics of 4th order QD-CPML from 20 °C to 100 °C under varied reverse bias voltages from 0 V to -5 V. The kinks in L-I curves at high V_{SA} is induced from nonlinear saturation effect of SAs. (b) Optical spectra evolutions with temperature increased from 20 °C to 100 °C. The operating current and reverse bias voltage at each temperature are slightly adjusted to achieve flat-top comb spectra.

To investigate an optimum operation window of 4th order CPML where stable 100 GHz spacing flat-top OFC can be generated, a wide range of operation conditions have been systematically mapped with I_g ranging from 50 mA to 250 mA and V_{SA} ranging from 0 V to -5 V at room temperature. The 3 dB optical bandwidth and pulse width are characterized using optical spectrum analyzer and autocorrelator (AC) in order to analyze the comb performance in the frequency and time domain, respectively. In order to characterize the 3 dB optical bandwidth of the OFCs, optical spectral mapping under different operating conditions is studied in Fig. 3(a). In Fig. 3(a), as the gain section current increased, the single comb spectral lobe started to split into dual-state operation. The spectra splitting may be caused by state filling [42] or spatial hole burning effect (SHB) [43], hence photons excited by two groups of InAs QDs with different group velocity are formed inside the cavity which leads to dual-state mode-locked condition or unlocked region at low reverse bias. Simultaneous with occurrence of dual-state region, the AC pulse traces also disappear at this unlocked region. It is noted that the spectra have unstable regions (I_g = 150 - 160 mA, 190 – 200 mA) where random modes appear, that lead to uneven comb spacings. These unstable comb regions are marked as gray area in Fig. 3(a), which is believed to be caused by strong mode competition within the dual-state region. Exceptionally, an ultra-wide optical comb spectrum is achieved at 180 mA (V_{SA} = -3 V) by perfect merging of two lobes of comb lines, however, the operation window is relatively narrow comparing to the stable flat-top comb region at higher injection current. Therefore, by further increase the injection current and reverse bias voltage, we have reached flat-top region above 210 mA, where the 3 dB bandwidth significantly broadened. This region is here defined as the optimum operation range of QD-CPML for ultra-broadband flat-top comb source.

OPTICAL PUBLISHING GROUP
Formerly OSA

The generation of broadband flat-top combs is the major focus in this paper for high capacity WDM applications. For the flat-top ML region discussed above, high resolution sweep of comb line counts within 3 dB optical bandwidth is performed over an optimum reverse bias range from 3 V to 4.5 V with magnified 0.1 V step and varying injection current from 210 mA to 250 mA under 1 mA step increment. As shown in Fig. 3(b), there is a 'riverway' like unlocked region separating the flat-top comb area, along the left 'riverbank', the comb spectral bandwidth reaches the maximum condition. Two dark red blocks show the best conditions which can generate 20 comb lines within 3 dB optical bandwidth.

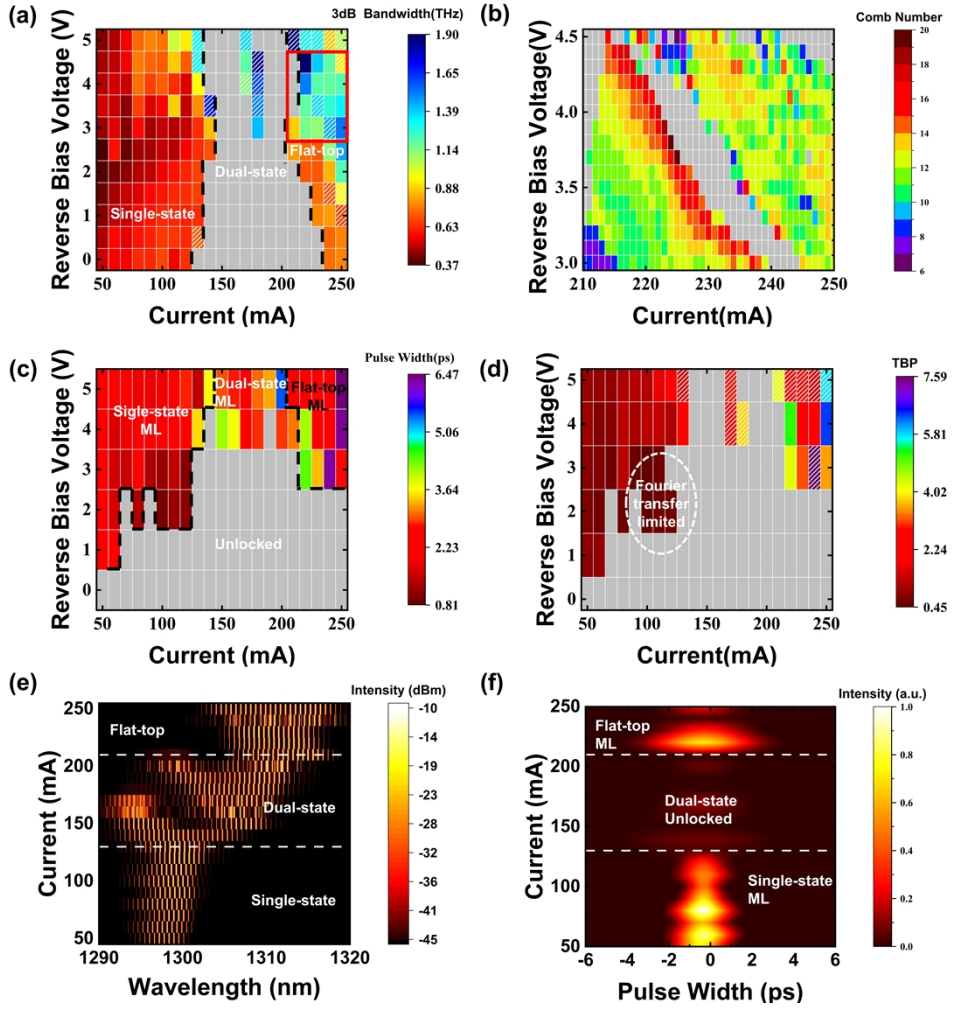

Fig. 3. 4th order QD-CPML (a) optical spectrum 3 dB bandwidth mapping as a function of SA reverse bias voltage ranging from 0 V to 5 V with 0.5 V step and injection current of gain sections varying from 50 mA to 250 mA with 10 mA step. (b) a precisely swept map of comb line numbers within 3 dB optical bandwidth as a function of SA reverse bias voltage varying from 3 V to 4.5 V with 0.1 V step and gain section injection current changing from 210 mA to 250 mA with 1 mA step (the mapping area corresponds to the red rectangular zone in (a)). (c) pulse width and (d) time-bandwidth product (TBP) mapping as a function of SA reverse bias voltage ranging from 0 V to 5 V with 1 V step and gain section injection current ranging from 50 mA to 250 mA with 10 mA step. (e) Optical spectra and (f) Pulse AC trace evolutions with injection current from 50 mA to 250 mA with 10 mA step at -3 V reverse bias voltage.

Three operation zones are distinguished here by analyzing the spectral envelope shapes, which are single-state region, dual-state region and flat-top region. In addition, the mapping results of pulse width is shown in Fig. 3(c), where the narrowest full width half maximum

(FWHM) of AC trace (dark red region) is ~810 fs at operating condition V_{SA} = -2 V, I_g = 100 - 120 mA, which is comparable to the state of art performance of two-section MLL [33,35]. No AC pulses or very weak pulses are observed in grey area of the mapping, hence this operating condition is defined as unlocked region. Furthermore, the time bandwidth product (TBP) values are then calculated and mapped in Fig. 3(d) using the data shown in Fig. 3(a) and 3(c). In the single-state ML region, the TBP value is normally below 1.2, except that very small TBP value of ~ 0.45 is achieved at 120 mA, which is close to the gaussian shape fourier transfer limited theoretical value of 0.44. This fourier transfer limited region is marked in Fig. 3(c).

As injection currents is elevated over 210 mA, the dual-state region were strongly suppressed, while merging back into single lobe comb spectra as shown in Fig. 3(e). Different from the gaussian-shape like spectrum, the optical spectrum is broadened to a rectangular shape with flat profiles thus the region is named as flat-top ML. The formation of flat-top profile is induced from the great compensation of increased Kerr nonlinearity at high carrier injection towards increased group velocity dispersion (GVD) across the enlarged spectral bandwidth. Similar mechanisms have been previously discussed theoretically and experimentally in single section MLLs [44-47]. The results are in line with significantly broadened AC pulse width of a few picosecond (Fig. 3(c)), indicating an enhanced dispersion process within flat-top MLL region compared with single-state MLL region.

To further investigate the ML evolution at fixed reverse bias voltage in both optical spectral and time domains, current dependent optical spectral and normalized pulse width evolution at V_{SA} = -3 V are plotted in Fig. 3(e) and Fig. 3(f), respectively. Right above the threshold current, the QD-CPML operates as single-state comb spectrum at injection current ranging from 50 mA to 120 mA, where the optical spectra are red shifted and broadened with increased current, eventually move into flat-top region above 210 mA. In the time domain (Fig. 3(f)), the pulses are getting narrower at towards injection current of 120 mA, where sub-picosecond pulse of 860 fs is detected. Further into the flat-top ML region, due to increased GVD, the pulse width is also extended to few picoseconds. Overall, the optical spectral mapping, pulse width mapping and TBP mapping are in good agreement, which give us clear guidance in operation condition selection for different application scenarios.

Under optimum operating condition of I_g = 224 mA and V_{SA} = -3.8 V, twenty 100 GHz spacing comb channels with 3 dB optical bandwidth of 11.5 nm are produced as shown in Fig. 4(a). It can be clearly observed that each comb line exhibits optical signal to noise ratio (OSNR) over 35 dB. To examine the performance of each comb channel, a tunable bandpass filter (EXFO XTM-50) is used together with an O-band Praseodymium-doped fiber amplifier (PDFA) (FiberLabs Inc. AMP-FL8611-OB-16) for overcoming the coupling and insertion loss. To note, the measured single channel optical power is approximately 1.7 mW without taking into account of coupling loss and insertion loss from OBPF (before coupling into OBPF). The frequency noise is characterized through a commercial homodyne system (OEwave 4000).

Fig. 4(b) shows the frequency noise spectra of 18 filtered comb lines. By fitting the white noises, the intrinsic Lorentz optical linewidths are estimated and plotted in Fig. 4(a). The average optical linewidth of 18 comb channels is approximately 440kHz which is one order of magnitude lower than reported conventional QD MLLs [33]. The narrow optical linewidth indicates the phases of individual comb lines are highly coherent through high-order mode locking. Furthermore, the relative intensity noise (RIN) spectra of each comb lines (PDFA amplified) and entire comb spectrum are both characterized. Fig. 4(c) shows that the 18 individual channels and whole comb spectrum have average RIN of -135 dB/Hz and -160 dB/Hz in the range from 0 – 20 GHz, respectively. Although there are approximately 25 dB/Hz degradation in RIN values for individual comb lines, the average

OPTICA PUBLISHING GROUP Formerly OSA

RIN values of each single sideband still meet the requirements for high-speed PAM-4 modulation [48] and WDM standards [29]. Moreover, the stability of each comb channel is tested using a wavelength meter (Thorlabs OSA 202C) in Fig. 4(d). The wavelength drift of 18 combs is less than 200 MHz for 10 minutes monitoring. For extended time stability test that is also applied to a comb channel at 1317.69 nm, the wavelength variation is less than 1 GHz as shown in the inset of Fig. 4(d). All the measurements are under free-running conditions, it is believed that the combs can be further stabilized by wavelength locker design with a feedback control loop [49].

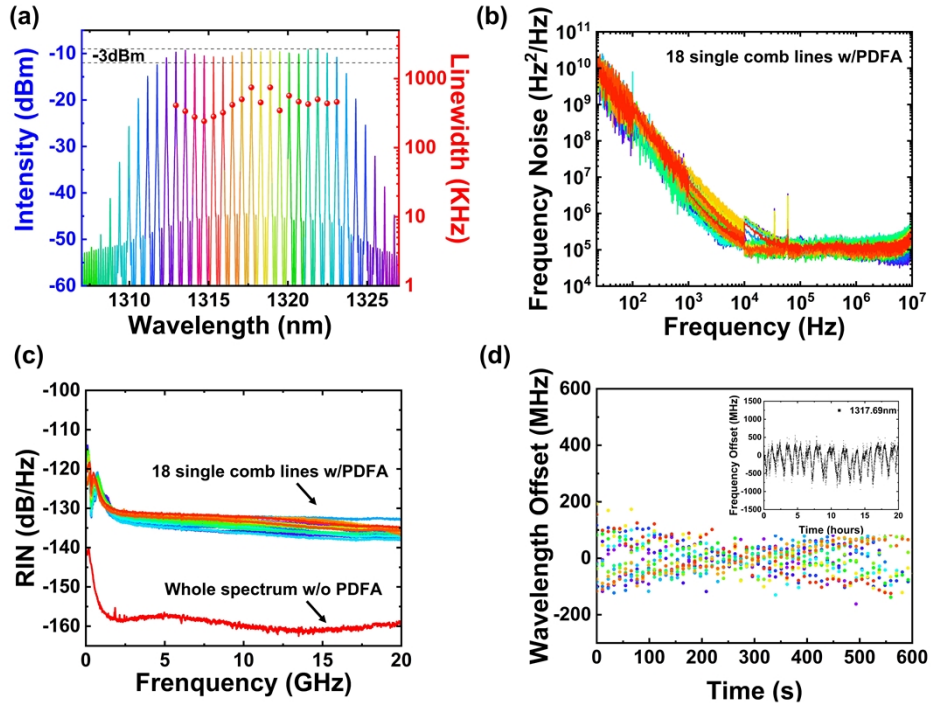

Fig. 4. (a) Optical spectrum of flat top QD-CPML under optimized bias condition of I_g = 224 mA and V_{SA} = -3.8 V. (b) Optical linewidth of the frequency noise spectra from 18 filtered comb lines. (c) Relative intensity noise (RIN) of 18 filtered individual comb lines and the whole laser. (d) wavelength stability of 18 comb lines over 10 minutes and a single comb line wavelength offset over 20 hours (inset). (b), (c) and (d) are characterized at the same set of operating conditions as in (a).

High-speed external modulation of the 4th order CPML is demonstrated by evaluating the eye diagram performance of the laser. The large signal modulation experimental setup for QD comb laser is shown in Fig. 5(a). The CPML is operated at optimum flat-top conditions as discussed above, then coupled into an optical band pass filter (OBPF) to select individual comb channels as optical carriers. Single channel at 1321.28 nm is selected for testing to show the typical performance. By adjusting the amplification current of PDFA, the carrier is amplified to 10 dBm and coupled into a 40 GHz lithium niobate (LN) Mach–Zehnder modulator (MZM) (iXblue MX1300-LN-40) for data modulation. The modulation signals are produced from an arbitrary waveform generator (AWG) (Keysight M8194A) with a 2^7-1 pseudo-random binary sequence (PRBS) patterns. The signals are amplified to ~3 V peak-to-peak output power through a 38 GHz broadband RF amplifier (SHF 806E). The external modulated signals are then sent to an optical sampling oscilloscope (OSC) (Tektronix DSA8300) to show the eye diagram. Fig. 5(b) and 5(c) show the measured eye diagrams for 70 Gbits/s NRZ and 40 GBaud/s PAM-4 modulation format with extinction

ratio of 4.4 dB and 6.4 dB, respectively. To note, the modulation speed used here is limited by the maximum bandwidth of O-band LN modulator, which is expected to reach over 100 Gb/s with additional advanced digital signal process [33] and large bandwidth EO modulator [50]. Here, all comb channels here have been measured through high-speed modulation, which exhibit similar eye diagrams at 80 Gbits/s. Since there are 20 channels in total within the 3 dB optical bandwidth, the 100 GHz spacing flat-top OFC can be practically used to achieve 1.6 Tbit/s data transmission using 40 Gbaud/s PAM-4 modulation format.

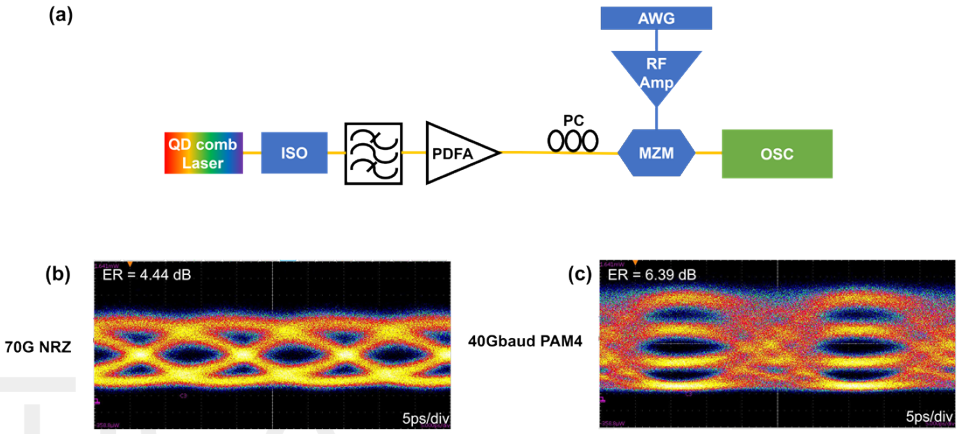

Fig. 5. (a) Experimental setup used to measure B2B NRZ and PAM-4 transmission characteristics of QD-CPML, including ISO, optical isolator; OBPF, optical bandpass filter; PDFA, Praseodymium-doped fiber amplifier; PC, polarization controller; AWG, arbitrary waveform generator; RF Amp, RF amplifier; MZM, Mach-Zehnder modulator; OSC, optical sampling oscilloscope. (b) 70G NRZ and (c) 40Gbaud PAM-4 optical eye diagram using comb line at 1321.28nm.

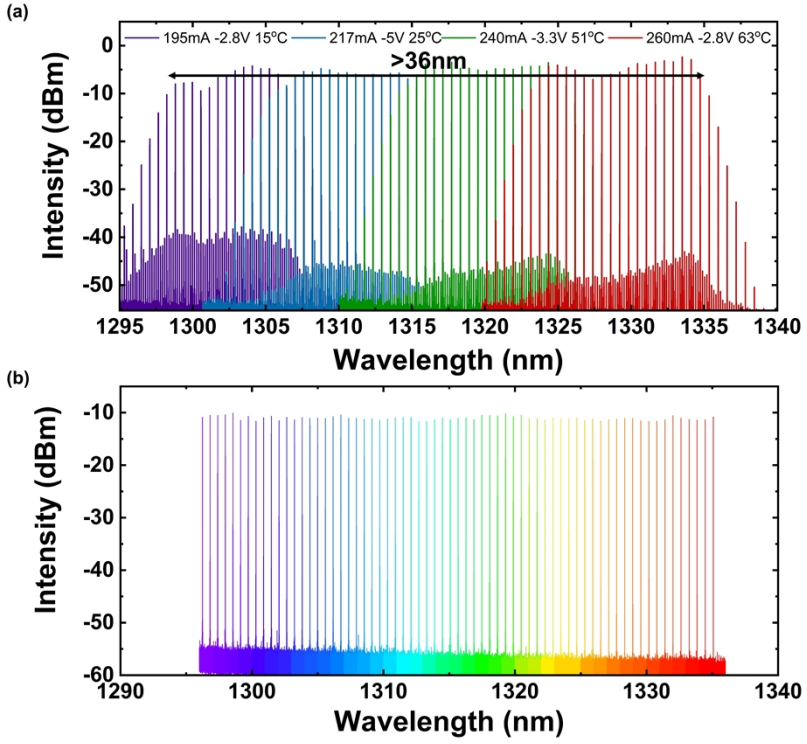

OPTICA PUBLISHING GROUP Formerly C

Fig. 6. (a) Combined optical spectra of 4th order QD-CPML for extended optical bandwidth under the temperature of 15°C, 25°C, 51°C and 63°C (Purple line: I_g=195 mA, V_{SA}= -2.8 V; Blue line: I_g=217 mA, V_{SA}= -5 V; Green line: I_g=240 mA, V_{SA}= -3.3 V; Red line: I_g=260 mA, V_{SA}= -2.8 V). The maximum channel counts can reach 60 comb lines within 6 dB optical bandwidth. (b) Combined optical spectra of all 60 channels with filtering of each channel via OBPF.

The total transmission bandwidth can also be enhanced in aspect of optical bandwidth. Taking advantage of temperature resilience properties of QD lasers, the optical spectrum could be extended by combining output optical spectra from QD laser array that each laser is operated at properly designed temperature. The proof-of-concept experiment has been performed by adjusting operation temperature of a QD-CPML to seamlessly combine and extend the optical spectra. As shown in Fig. 6, the 6 dB optical bandwidth of OFCs are successfully extended to 36 nm with temperature varying from 15°C to 63°C. The broadened optical bandwidth includes sixty 100 GHz spacing OFCs which has potential of increasing the data transmission capacity further to 4.8 Tbit/s.

4. CONCLUSIONS

We have successfully demonstrated an O-band 100 GHz grid 4th order QD-CPML with a record high 3 dB optical bandwidth of 11.5 nm. Taking advantage of temperature insensitivity of QDs, the laser could generate flat-top OFCs with average 3 dB bandwidth over 10 nm within wide temperature range from 20°C to 80°C. Sophisticated analyses of high order CPML are included in this work, both Fourier transfer limited sub-picosecond pulses and flat-top comb can be generated from the QD-CPML at different ML regions. The flat-top comb laser shows excellent integrated average RIN values of the entire spectrum and 18 filtered channels at -135 dB/Hz and -160 dB/Hz, respectively. We have achieved 18 flat-top comb lines with an average optical linewidth of 440 kHz which is the lowest value for high order CPM semiconductor laser to the best of our knowledge. Without active feedback loop control, the free running QD-CPML has wavelength offset value less than 1 GHz over 20 hours reliability test. Twenty comb lines are selected as optical carriers with 1.6 Tbit/s transmission capability is demonstrated by modulating each channel with 40 GBaud/s PAM-4 format. An extended optical bandwidth solution is proposed here with 36 nm broadband spectrum containing maximum 60 channels at 100 GHz grid, which is a promising approach to achieve 4.8 Tbit/s data transmission. As a weight and power (SWaP) multi-wavelength source solution, we expect this high bandwidth flat-top QD-CPML would be widely used in WDM systems, optical interconnects and photonic neural networks.

OPTICA PUBLISHING GROUP Formerly OSA

Funding.

This research was funded by National Key Research and Development Program of China (2021YFB2800400), National Natural Science Foundation of China (Grant No. 61975230, 62005308). Ting Wang was supported by the Youth Innovation Promotion Association of CAS (No. 2018011).

Disclosures.

The authors declare no conflicts of interest.

Acknowledgments.

The authors would like to thank Mr. Mingchen Guo, Miss Shujie Pan and Miss Yiou Cui for their constructive contributions in device fabrications and measurements.

†These authors contributed equally to this work.

REFERENCES

1. R. Wu, V. R. Supradeepa, C. M. Long, D. E. Leaird, and A. M. Weiner, "Generation of very flat optical frequency combs from continuous-wave lasers using cascaded intensity and phase modulators driven by tailored radio frequency waveforms," Opt. Lett. **35**, 3234-3236 (2010).

2. M. Y. Xu, M. B. He, Y. T. Zhu, S. Y. Yu, and X. L. Cai, "Flat Optical Frequency Comb Generator Based on Integrated Lithium Niobate Modulators," J. Light. Technol. 1-1 (2021).
3. S. Liu, K. Wu, L. Zhou, L. Lu, B. Zhang, G. Zhou, and J. Chen, "Optical Frequency Comb and Nyquist Pulse Generation With Integrated Silicon Modulators," IEEE J. Sel. Top. Quantum Electron. **26**, 1-8 (2019).
4. P. Del'Haye, A. Schliesser, O. Arcizet, T. Wilken, R. Holzwarth, and T. J. Kippenberg1, "Optical frequency comb generation from a monolithic microresonator," Nature **450**, 1214-1217, (2007).
5. T. J. Kippenberg and R. Holzwarth S. A. Diddams, "Microresonator-based optical frequency combs," Science **332**, 555-559 (2011).
6. M. G. Suh and K. J. Vahala, "Soliton microcomb range measurement," Science 359, 884–887 (2018).
7. W. L. Weng, A. Kaszubowska-Anandarajah, J. J. He, P. D. Lakshmijayasimha, E. Lucas, J. Q. Liu, P. M. Anandarajah, and T. J. Kippenberg, "Gain-switched semiconductor laser driven soliton microcombs," Nat. Comm. **12**, 1425 (2021).
8. R. Zhou, S. Latkowski, J. O'Carroll, R. Phelan, L. P. Barry, and P. Anandarajah, "40nm wavelength tunable gain-switched optical comb source," Opt. Express **19**, B415-B420 (2011).
9. E. U. Rafailov, M. A. Cataluna, and W. Sibbett, "Mode-locked quantum-dot lasers," Nat. Photon. **1**, 395-401 (2007).
10. A. Aboketaf, A. Elshaari, and S. Preble, "Optical time division multiplexer on silicon chip," Opt. Express **18**, 13529-13535 (2010).
11. D. Kong, H. Xin, K. Kim, Y. Liu, L. K. Oxenloewe, P. Dong, and H. Hu, "Intra-datacenter interconnects with a serialized silicon optical fre-quency comb modulator," J. Lightwave. Technol. **38**, 4677–4682 (2020).
12. Z. Lu, J. Liu, S. Raymond, P. Poole, P. Barrios, and D. Poitras, "312-fs pulse generation from a passive C-band InAs/InP quantum dot mode-locked laser," Opt. Express **16**, 10835-10840 (2008).
13. J. Liu, Z. Lu, S. Raymond, P. Poole, P. Barrios, and D. Poitras, "Dual-wavelength 92.5 GHz self-mode-locked InP-based quantum dot laser," Opt. Lett. **33**, 1702-1704 (2008).
14. Z. G. Lu, J. R. Liu, C. Y. Song, J. Weber, Y. Mao, S. D. Chang, H. P. Ding, P. J. Poole, P. J. Barrios, D. Poitras, S. Janz, and M. O'Sullivan, "High performance InAs/InP quantum dot 34.462-GHz C-band coherent comb laser module," Opt. Express **26**, 2160-2167 (2018).
15. X. Huang, A. Stintz, H. Li, L. F. Lester, J. Cheng, and K. J. Malloy, "Passive mode-locking in 1.3 μm two-section InAs quantum dot lasers," Appl. Phys. Lett **78**, 2825-2827 (2001).
16. B. Dong, H. Huang, J. Duan, G. Kurczveil, D. Liang, R. Beausoleil, and F. Grillot, "Frequency comb dynamics of a 1.3um hybrid-silicon quantum dot semiconductor laser with optical injection," Opt. Lett. **44**, 5755-5758 (2019).
17. J. Duan, H. Huang, B. Dong, J. C. Norman, Z. Zhang, J. E. Bowers, and F. Grillot, "Dynamic and nonlinear properties of epitaxial quantum dot lasers on silicon for isolator-free integration," Photonics Res. **7**, 1222-1228 (2019).
18. J. J. Chen, Z. H. Wang, W. Q. Wei, T. Wang, and J. J. Zhang, "Sole Excited-State InAs Quantum Dot Laser on Silicon with Strong Feedback Resistance," Front. Mater. **8**, 163 (2021).
19. J. Kwoen, B. Jang, K. Watanabe, and Y. Arakawa, "High-temperature continuous-wave operation of directly grown InAs/GaAs quantum dot lasers on on-axis Si (001)," Opt. Express **27**, 2681-2688 (2019).
20. J. C. Norman, D. Jung, Z. Y. Zhang, Y. T. Wang, S. T. Liu, C. Shang, R. W. Herrick, W. W. Chow, A. C. Gossard, and J.E. Bowers, "A Review of High-Performance Quantum Dot Lasers on Silicon," IEEE J. Quantum Electron. **55**, 1-11 (2019).
21. S. Chen, W. Li, J. Wu, Q. Jiang, M. Tang, S. Shutts, S.N. Elliott, A. Sobiesierski, A. J. Seeds, I. Ross, and P.M. Smowton, "Electrically pumped continuous-wave III–V quantum dot lasers on silicon," Nat. Photon. **10**, 307–311 (2016).
22. A. Y. Liu, C. Zhang, J. Norman, A. Snyder, D. Lubyshev, J. M. Fastenau, A. W. Liu, A. C. Gossard, and J. E. Bowers, "High performance continuous wave 1.3 μm quantum dot lasers on silicon," Appl. Phys. Lett. **104**, 041104 (2014).
23. Z. H. Wang, W. Q. Wei, Q. Feng, T. Wang, and J. J. Zhang, "InAs/GaAs quantum dot single-section mode-locked lasers on Si (001) with optical self-injection feedback," Opt. Express **29**, 674-683 (2021).
24. W. Q. Wei, J. Y. Zhang, J. H. Wang, H. Cong, J. J. Guo, Z. H. Wang, H. X. Xu, T. Wang, and J. J. Zhang, "Phosphorus-free 1.5 μm InAs quantum-dot microdisk lasers on metamorphic InGaAs/SOI platform," Opt. Lett. **45**, 2042-2045 (2020).
25. W. Q. Wei, Q. Feng, J. J. Guo, M. C. Guo, J. H. Wang, Z. H. Wang, T. Wang, and J. J. Zhang, "InAs/GaAs quantum dot narrow ridge lasers epitaxially grown on SOI substrates for silicon photonic integration," Opt. Express **28**, 26555-26563 (2020).
26. Q. Feng, W. Q. Wei, B. Zhang, H. L. Wang, J. H. Wang, H. Cong, T. Wang, and J. J. Zhang, "O-Band and C/L-Band III-V Quantum Dot Lasers Monolithically Grown on Ge and Si Substrate," Appl. Sci. **9**, 385 (2019).
27. Z. C. Wang, K. V. Gasse, V. Moskalenko, S. Latkowski, E. Bente, B. Kuyken, and G. Roelkens, "A III-V-on-Si ultra-dense comb laser," Light Sci. Appl. **6**, 6260 (2017).
28. C. Kumar and R. Goyal, "Effect of Crosstalk in Super Dense Wavelength Division Multiplexing System using Hybrid Optical Amplifier," J. Opt. Commun. **40**, 347-351 (2019).
29. M. Sysak, J. Johnson, and D. Lewis, "CW-WDM MSA Technical Specifications Rev 1.0", CW-WDM MSA public document (2021).

OPTICA PUBLISHING GROUP Formerly OSA

30. Z. Zhang, R. Hogg, X. Lv, and Z. Wang, "Self-assembled quantum-dot superluminescent light-emitting diodes," Adv. Opt. Photon. **2**, 201-228 (2010).
31. V. Corral, R. Guzmán, C. Gordón, X. J. M. Leijtens, G. Carpintero, "Optical frequency comb generator based on a monolithically integrated passive mode-locked ring laser with a Mach–Zehnder interferometer," Opt. Lett. **41**, 1937-1940 (2016).
32. M. L. Davenport, S. T. Liu, and J. E. Bowers, "Integrated heterogeneous silicon/III–V mode-locked lasers," Photon. Res. **6**, 468-478 (2018).
33. S. T. Liu, X. R. Wu, D. Jung, J. C. Norman, M. J. Kennedy, H. K. Tsang, A. C. Gossard, and J. E. Bowers, "High-channel-count 20 GHz passively mode-locked quantum dot laser directly grown on Si with 4.1 Tbit/s transmission capacity," Optica **6**, 128-134 (2019).
34. S. J. Pan, J. O. Huang, Z. C. Zhou, Z. X. Liu, L. Ponnampalam, Z. Z. Liu, M. C. Tang, M. C. Lo, Z. Z. Cao, K. Nishi, K. Takemasa, M. Sugawara, R. Penty, I. White, A. Seeds, H. Y. Liu, and S. M. Chen, "Quantum dot mode-locked frequency comb with ultra-stable 25.5 GHz spacing between 20 °C and 120 °C," Photon. Res. **8**, 1937-1942 (2020).
35. L. P. Hou, Y. G. Huang, Y. H. Liu, R. K. Zhang, J. K. Wang, B. J. Wang, H. L. Zhu, B. Hou, B. C. Qiu, and J. H. Marsh, "Frequency comb with 100 GHz spacing generated by an asymmetric MQW passively mode-locked laser," Opt. Lett. **45**, 2760-2763 (2020).
36. G. Kurczveil, C. Zhang, A. Descos, D. Liang, M. Fiorentino and R. Beausoleil, "On-chip hybrid silicon quantum dot comb laser with 14 error-free channels, " IEEE International Semiconductor Laser Conference (ISLC), pp. 1-2 (2018).
37. G. Kurczveil, A. Descos, D. Liang, M. Fiorentino, and R. Beausoleil, "Hybrid silicon quantum dot comb laser with record wide comb width, " OSA FiO_LS Virtual Conference, paper FTu6E.6 (2020).
38. Y. Li, F. Chiragh, Y. Xin, C. Lin, J. Kim, C. Christodoulou, and L. Lester, "Harmonic mode-locking using the double interval technique in quantum dot lasers," Opt. Express **18**, 14637-14643 (2010).
39. H. Y. Liu, S. L. Liew, T. Badcock, D. J. Mowbray, M. S. Skolnick, S. K. Ray, T. L. Choi, K. M. Groom, B. Stevens, F. Hasbullah, and C.Y. Jin, "p -doped 1.3μm InAs⁄GaAs quantum-dot laser with a low threshold current density and high differential efficiency," Appl. Phys. Lett. **89**, 073113 (2006).
40. J. Z. Huang, W. Q. Wei, J. J. Chen, Z. H. Wang, T. Wang, and J. J. Zhang, "P-doped 1300 nm InAs/GaAs quantum dot lasers directly grown on SOI substrate," Opt. Lett. (2021) (in Press).
41. J. K. Mee, R. Raghunathan, D. Murrell, A. Braga, Y. Li and L. F. Lester, Novel Optical Systems Design and Optimization XVII. Vol. 9193. International Society for Optics and Photonics, 2014.
42. S. G. Li, Q. Y. Gong, Y. F. Lao, H. Yang, S. Gao, P. Chen, Y. G. Zhang, S. L. Feng, and H. L. Wang, "Two-color quantum dot laser with tunable wavelength gap," Appl. Phys. Lett. **95**, 251111 (2009).
43. M. Charis, C. Simos, I. Simos, S. Mikroulis, I. Krestnikov, and D. Syvridis, "Pulse width narrowing due to dual ground state emission in quantum dot passively mode locked lasers," Appl. Phys. Lett. **96**, 211110 (2010).
44. J. Hillbrand, D. Auth, M. Piccardo, N. Opačak, E. Gornik, G. Strasser, F. Capasso, S. Breuer, and B. Schwarz, "In-Phase and Anti-Phase Synchronization in a Laser Frequency Comb," Phys. Rev. Lett. **124**, 023901 (2020).
45. N. Opačak and B. Schwarz, "Theory of frequency-modulated combs in lasers with spatial hole burning, dispersion, and kerr nonlinearity," Phys. Rev. Lett. **123**, 243902 (2019).
46. S.P. Duill, S.G. Murdoch, R.T. W atts, R. Rosales, A. Ramdane, P. Landais, and L.P. Barry, "Simple dispersion estimate for single-section quantum-dash and quantum-dot mode-locked laser diodes," Opt. Lett. **41**, 5676-5679 (2016).
47. R. Rosales, S. G. Murdoch, R.T. Watts, K. Merghem, A. Martinez, F. Lelarge, A. Accard, L.P Barry, and A. Ramdane, "High performance mode locking characteristics of single section quantum dash lasers," Opt. Express **20**, 8649-8657 (2012).
48. N. Eiselt, H. Griesser, M. Eiselt, W. Kaiser, S. Aramideh, J. Olmos, I. Monroy, and J. Elbers, "Real-Time 200 Gb/s (4×56.25 Gb/s) PAM-4 Transmission over 80 km SSMF using Quantum-Dot Laser and Silicon Ring-Modulator," Optical Fiber Communication Conference, 2017, vol. Part F40-O, p. W4D.3
49. Z. G. Lu, J. R. Liu, C. Y. Song, J. Weber, Y. Mao, S. D. Chang, H. P. Ding, P. J. Poole, P. J. Barrios, D. Poitras, S. Janz, and M. O'Sullivan, "High performance InAs/InP quantum dot 34.462-GHz C-band coherent comb laser module." Opt. Express **26**, 2160-2167 (2018).
50. M. B. He, M. Y. Xu, Y. X. Ren, J. Jian, Z. L. Ruan, Y. S. Xu, S. Q. Gao, S. H. Sun, X. Q. Wen, L. D. Zhou, L. Liu, C. J. Guo, H. Chen, S. Y. Yu, L. Liu, and X. L. Cai, "High-performance hybrid silicon and lithium niobate Mach–Zehnder modulators for 100 Gbits^{-1} and beyond," Nat. Photon. **13**, 359–364 (2019).

OPTICA PUBLISHING GROUP Formerly OSA